JOURNAL OF MATERIALS SCIENCE 27 (1992) 2326–2334

Metallurgical structure and alkali leaching of the Al/Al_3Ni eutectic

P. COLIN, S. HAMAR-THIBAULT, J. C. JOUD
LTPCM-ENSEEG, BP 75, 38402 Saint Martin d'Hères, Cédex, France

Raney-Nickel catalysts were prepared by aluminium leaching out of aluminium-rich binary Al–Ni alloys. In order to understand the behaviour of $NiAl_3$ during alkali leaching, different metallurgical structures of the Al/Al_3Ni eutectic were prepared as precursor alloys. This eutectic showed a fibrous morphology with Al_3Ni fibres embedded in an aluminium matrix. After alkali leaching, transmission electron microscopy observations showed that the fibrous microstructure was retained. The fibres were formed with small nickel crystallites. During the early stages of leaching, a reaction front was observed which remained parallel to the Al/Al_3Ni interface.

1. Introduction

Since the advent of Raney–Nickel catalysts about 60 years ago, nickel catalysts have been widely used for liquid-phase hydrogenation reactions. Although Raney–Nickel catalysts were prepared from Al–Ni metallic alloys, only a few investigations have been done on the influence of the metallurgical structure of the precursor alloys upon the catalytic properties [1–4].

Commercial Raney–Ni catalysts were often prepared from Ni–Al (50–50 wt %) alloys by the leaching out of aluminium. As could be expected from examination of the Ni–Al binary equilibrium phase diagram [5], and the peritectic formation of the binary phases, Ni_2Al_3 (hexagonal lattice), $NiAl_3$ (orthorhombic lattice) and $Al/NiAl_3$, eutectic phases were always present in the Raney precursor alloys [6, 7]. By alkali leaching, the less noble metal aluminium was preferentially extracted from the binary phases, and a porous structure of the catalytically active nickel metal was produced. It is known that the reactivity of the binary phases increases with aluminium content. The Al/Al_3Ni eutectic alloy leaches more rapidly than Al_3Ni, which leaches more rapidly than Ni_2Al_3 [1, 8, 9].

In recent years, interest (from the catalytic point of view) in the pure Ni_2Al_3 and $NiAl_3$ compounds, and in the $Al/NiAl_3$ eutectic alloy, has increased. A large amount of work has been concerned with the $NiAl_3$ intermetallic compound which seems more reactive than Ni_2Al_3 and often shows better catalytic properties. Brooks *et al.* [10] and Lemkey *et al.* [11] prepared Raney–Ni catalysts from the eutectic composition. In this case aluminium leaching produced Raney–Ni catalysts in the form of unsupported skeletal fibres.

In order to understand the leaching process, some authors have studied the selective leaching of pure $NiAl_3$ and Ni_2Al_3 compounds in an alkali medium [12]. The aims of the present investigation were to study, at high resolution level, the morphologies of Al–Ni alloys in the eutectic range and the leaching behaviour of Al/Al_3Ni eutectic, particularly the structure of the active nickel phase formed from the $NiAl_3$ fibres.

Two metallurgical methods with different cooling rates were used to prepare precursor alloys with a fibrous microstructure: quenching from the liquidus and unidirectional solidification. The microstructure of the precursor alloys and their behaviour in alkali solution were characterized by scanning (SEM) and transmission (TEM) electron microscopy and analysed by energy dispersive X-ray analysis (EDX–STEM).

2. Experimental procedure

2.1. Alloy preparation

The Ni–Al eutectic alloys were synthesized by referring to the Hansen diagram [5], where the eutectic composition was reported to be at 5.7 wt % Ni (2.7 at %).

The initial alloys were prepared from pure elemental aluminium and nickel (99.99%). Accurately weighed components of each element were either melted in an induction furnace in a graphite crucible or arc-melted in an argon atmosphere using a non-consumable tungsten electrode. This latter operation was repeated two or three times to ensure homogenization of these samples. It was verified that no important losses of elements had occurred during sample preparation. Alloys compositions are given in atomic per cent.

Unidirectional solidification (US) has been used with a solidification rate close to 20 cm h^{-1} to produce ingots of about 8 mm diameter and up to 30 cm long. Details of this apparatus were presented in a previous paper [13]. Samples were then annealed at

0022–2461

different temperatures between 500 and 600 °C, for different times under an argon atmosphere in an alumina tube. The temperature was controlled using a thermocouple and the homogeneous zone in the centre of the furnace was determined.

2.2. Alkali-leaching of the alloys

Pieces with the same dimensions were leached in a large excess of a 6 N sodium hydroxide solution at room temperature for times close to 30 min. The temperature of the solution always remained below 30 °C. At this temperature Ni_2Al_3 was unreactive, $NiAl_3$ rapidly yielded porous nickel and the $Al/NiAl_3$ was more reactive. After 30 min, the eutectic structure became friable and disintegrated. The leached samples were carefully washed with distilled water and ethanol. Because the samples were pyrophoric, they were kept in distilled water to avoid any contact with air.

2.3. Investigative methods

Characterization was performed on the samples before and after different leaching times. Leached samples were introduced into the working chamber under alcohol and the liquid was then removed by pumping.

The alloys were first examined by SEM (Jeol-JSM 35SF) after being cut mechanically with a high concentration diamond wafering blade (Buehler Isomet). The undirectionally solidified samples were cut transversally and longitudinally then mechanically polished with metallographic abrasive discs and an alumina suspension.

More accurate observations were performed by TEM (Jeol-JEM 200 CX). The samples were first thinned down using an ion beam (Gatan Dual Ion Mill Model 600) until a small hole appeared. This procedure has been used to obtain very thin areas. Alkali leaching on these thin areas allowed the early stages of aluminium removal to be followed. TEM observations were performed on the same thin sample before and after leaching. Energy dispersive X-ray (EDX) microanalyses with a resolution of 1.5 nm at sample level were carried out on a VG-HB5-STEM coupled with a Tracor analyser.

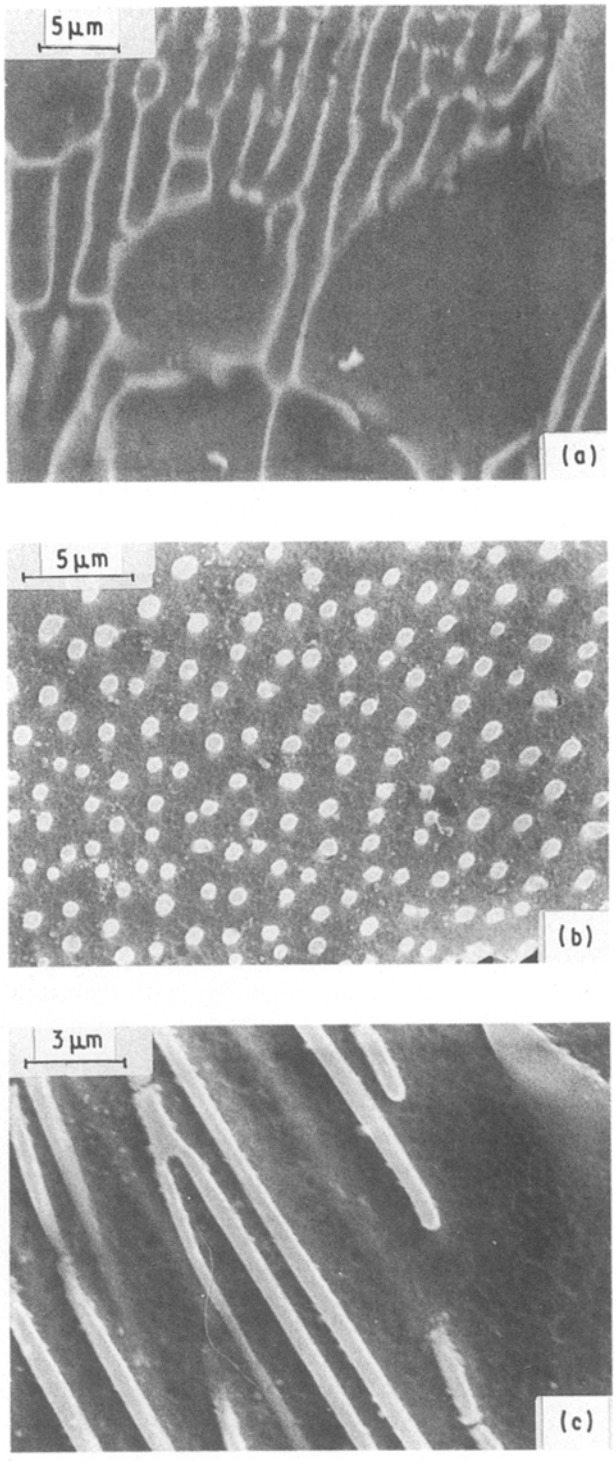

Figure 1 SEM images of the eutectic alloy (Ni = 5.7 wt %): (a) alloy quenched for liquidus; (b) transverse section of the unidirectionally solidified alloy; (c) longitudinal section of the unidirectionally solidified alloy. Branching is clearly shown.

3. Results

3.1. Microstructure and solidification behaviour

Binary Al–5.7 wt % Ni alloy prepared in the induction furnace showed a completely eutectic structure. On the other hand, the same alloy prepared by arc melting showed that about 10% of the aluminium solidified as primary dendrites. Moreover, the amount of primary aluminium dendrites depended on the location in the ingot and was larger in the external part than in the internal zones of the ingot, indicating some influence of cooling rate on the eutectic composition. As seen in Fig. 1a, around these primary dendrites, a large amount of nickel was rejected. A discontinuous halo of $NiAl_3$ was formed and the eutectic $Al/NiAl_3$ was then nucleated on this $NiAl_3$ phase.

This type of solidification process produced non-uniform fibres of $NiAl_3$ embedded in a large amount of aluminium. The mean diameter was around 0.2 µm but with a large distribution of diameters. The inter-fibre spacing value, λ (distance between two neighbouring fibre centres), was measured to be ~ 2 µm. The microstructure of unidirectionally solidified eutectic ($R = 18\ \text{cm h}^{-1}$, $50\ \mu\text{m s}^{-1}$) is shown in

Fig. 1b. Under these experimental conditions, the sample exhibited a cellular structure.

The $NiAl_3$ phase appeared as rods as shown on the TEM image of a transverse section (Fig. 2a). The fibres were uniform in shape and size. The area of more than 300 fibres was determined. The average diameter was calculated assuming that the fibres were circular (0.65 ± 0.10 μm). The distribution of fibre radius followed a Gauss graph centred on the average value. The minimum and maximum values were, respectively, 0.2 and 1 μm. Only 6% of the fibres had a diameter less than 0.5 μm and 9% a diameter larger than 0.8 μm. The smallest fibres were formed either by branching of large $NiAl_3$ fibres, as seen in the longitudinal section presented in Fig. 2c, or by the growth of new nuclei, as reported by Hertzberg *et al.* [14]. The largest fibres were always located at the cellular interfaces and showed tendency to exhibit small facets. The mean interfibre spacing, λ, determined on a transverse section, was around 1.6 ± 0.5 μm with a solidification rate of 18 cm h^{-1}.

TEM observations of samples of the eutectic composition, prepared by rapid solidification using the melt-spinning process, showed that the dispersed intermetallic phase was not $NiAl_3$. The diffraction patterns were indexed with a new metastable Ni_2Al_9 phase, isomorphous with the monoclinic Co_2Al_9 phase [15].

3.2. Crystallographic structure of the eutectic

Under our solidification conditions (with the exception of melt-spun alloys), the eutectic was well defined with the two phases: fcc aluminium and orthorhombic $NiAl_3$ (Pbnm, DO_{11}) lattices as seen on the superimposed electron diffraction patterns presented in Fig. 2 obtained from transverse sections in unidirectionally solidified alloys. Transverse sections were always indexed as (0 0 1) planes of the cubic aluminium phase. The aluminium matrix was oriented with one ⟨0 0 1⟩ direction parallel to the heat flow. On the contrary, the growth direction of the Al_3Ni fibres was around the ⟨0 0 1⟩ direction and varied from one point of the section to another by about 15°. The orientation relationship could be described as

growth direction ⟨0 0 1⟩$NiAl_3$//⟨0 0 1⟩Al
with (1 3 0) //(1 0 0)
and (2 1 0) //(0 1 0)

In as-cast alloys, no faceting of the fibres was observed, while in unidirectionally solidified alloys, most $NiAl_3$ fibres were round, but near the boundaries of the eutectic cells some faceted fibres could be observed. In order to promote this faceting, eutectic samples were treated at high temperature.

In quenched alloys, the eutectic structure consisted originally of regular rods of $NiAl_3$ (average diameter 0.65 μm). After annealing for 90 h at 600 °C (40 °C below the eutectic temperature) the microstructure had changed substantially. The regular distribution was lost and on transverse sections, two types of fibre were observed: small round fibres and large faceted ellipses showing small facets.

The smallest fibres remained almost circular with a mean diameter of 2.0 ± 0.5 μm. A faceted fibre is

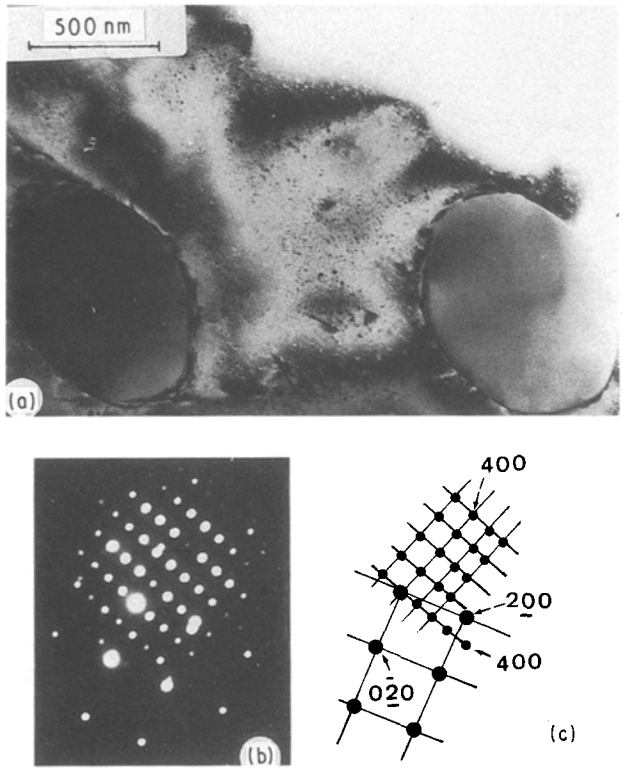

Figure 2 TEM images of the unidirectionally solidified eutectic: (a) round $NiAl_3$ fibre; (b) superimposed diagram pattern ⟨0 0 1⟩$NiAl_3$//⟨0 0 1⟩ Al; (c) key diagram (○) Al, (●) $NiAl_3$.

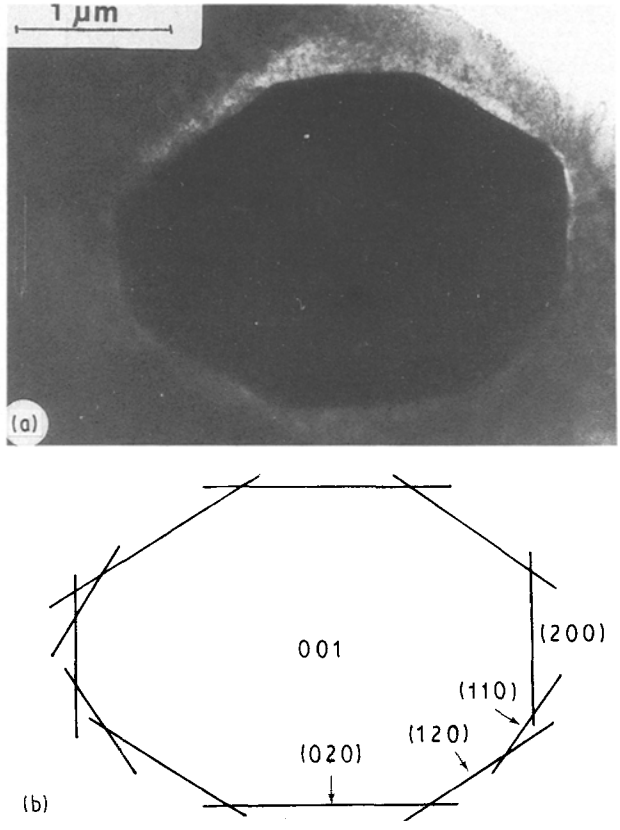

Figure 3 TEM images of the annealed eutectic alloy (600 °C, 90 h): (a) "round" fibre; (b) plane indexing.

shown in Fig. 3a and the interface planes are indexed. In this family, the fibres were limited with (0 2 0), (1 2 0) and (2 0 0) planes. (1 1 0) planes were sometimes noted.

Around 20% $NiAl_3$ fibres belong to a second class. The fibres were no longer round but showed a large degree of anisotropy with a cross-section showing an elliptical shape. The mean minor axis was 2.6 ± 0.1 μm. The length was between 3 and 5 μm. These elongated fibres appeared as platelets. The interfaces parallel to the large axis between aluminium and $NiAl_3$ were formed of two parallel planes belonging to the {0 2 0} family of the Ni_3Al phase and separated by at least 2 μm. At the interfaces parallel to the small axis, faceting could also be observed and the (1 1 0) and (2 0 0) planes were indexed. In some cases (1 2 0) planes were also observed. Fig. 4 shows a typical elongated faceted fibre.

From these results, the two-dimensional coarsening of the fibres seemed to occur in two steps: first an isotropic coarsening of round fibres until a mean diameter of about 2 μm was reached, then an anisotropic coarsening occurred and the fibres could be described as faceted ellipses with a major axis parallel to the ⟨1 0 0⟩ direction of $NiAl_3$.

3.3. Alkali leaching of the eutectic structure

The Al/Al_3Ni eutectic was very reactive in alkali solution. Aluminium was leached out rapidly even at room temperature in NaOH 6 mol l^{-1}. Initially, selective removal of the aluminium matrix occurred, keeping unchanged the fibrous structure of the $NiAl_3$ fibres, as shown in Fig. 5.

More accurate observations by TEM showed that extraction of aluminium atoms also occurred in the intermetallic $NiAl_3$ phase. Aluminium leaching out of the $NiAl_3$ compound lead to the formation of porous nickel fibres (Fig. 6). These leached fibres appeared with a sponge-like structure composed of small nickel crystallites. After 10 min leaching, selected-area diffraction patterns performed on these porous fibres were typical of the face centred cubic structure of the nickel lattice, as shown in the diffraction pattern inserted in Fig. 6. The nickel crystallites were not oriented at random and a ⟨1 1 0⟩ direction of the fcc cell of nickel was indexed.

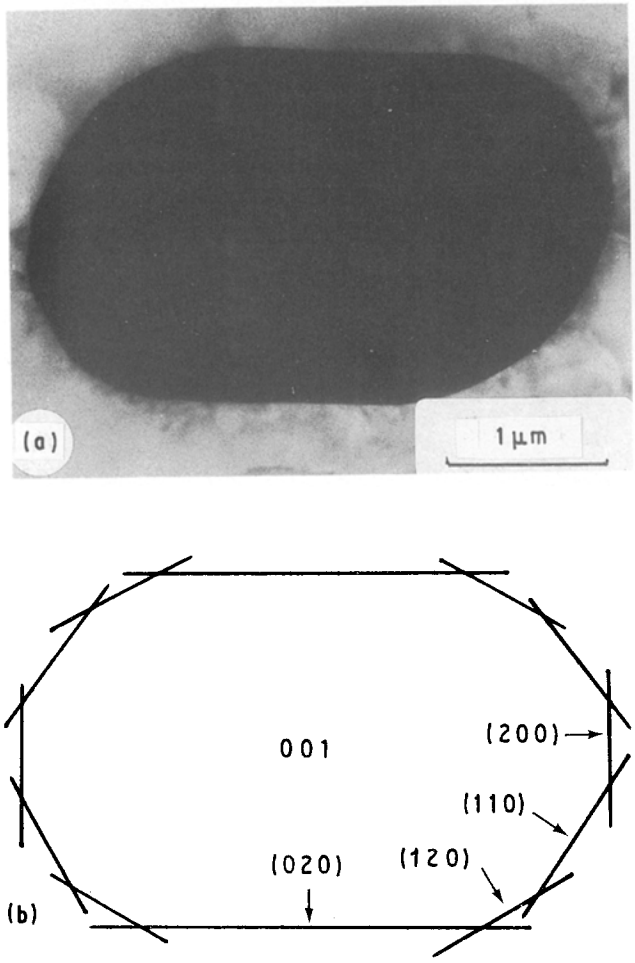

Figure 4 TEM images of the annealed eutectic alloy (600 °C, 90 h): (a) "elongated" fibre; (b) plane indexing.

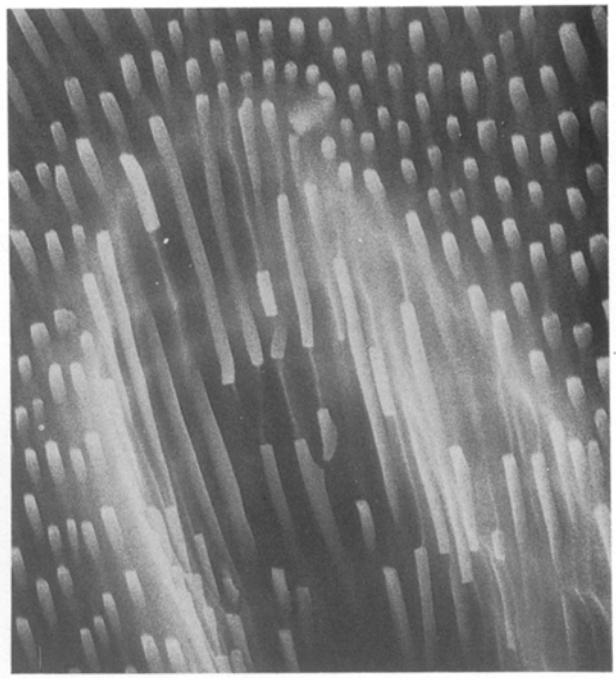

Figure 5 SEM image showing that the fibrous structure is retained after alkali leaching (30 min, 6 N NaOH).

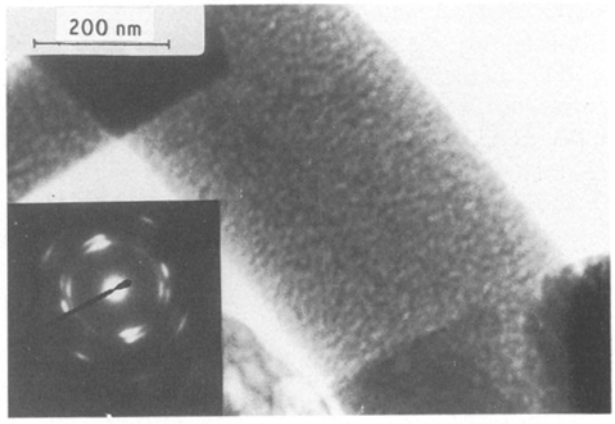

Figure 6 TEM image of a porous fibre and diffraction pattern ⟨1 1 0⟩ showing the texture of the nickel residue obtained after alkali leaching.

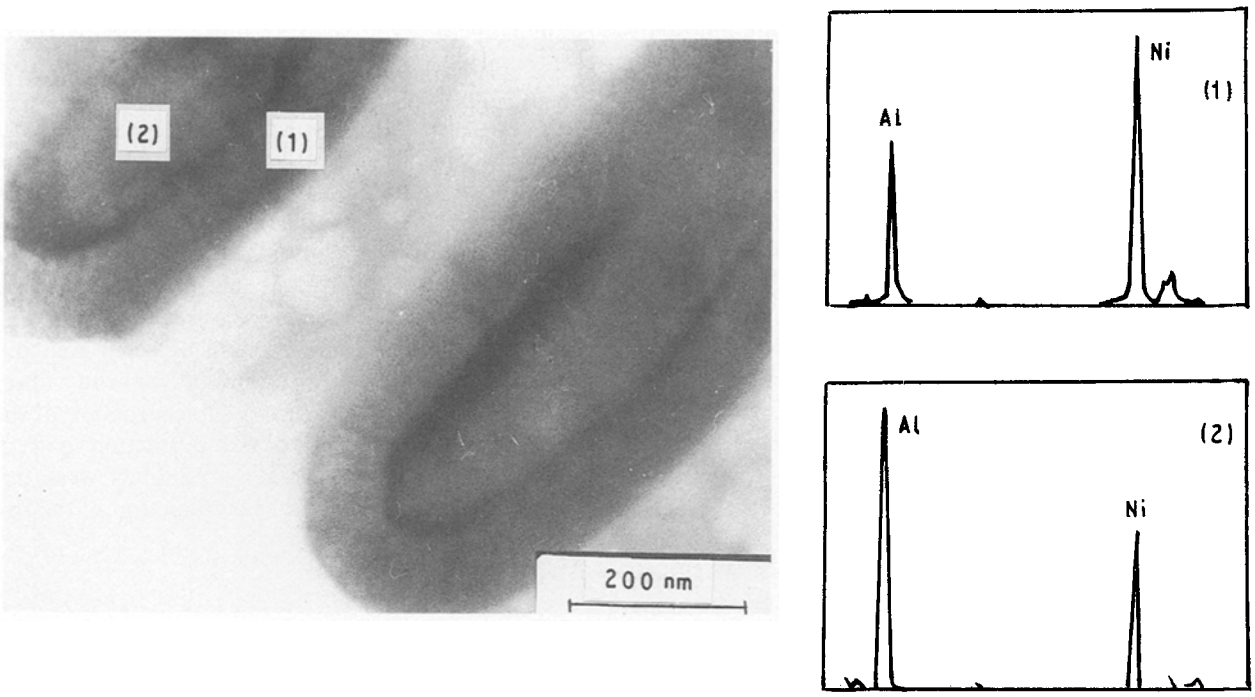

Figure 7 STEM/EDX analysis of the $NiAl_3$ fibres after alkali leaching (15 s, 6 N NaOH at room temperature) showing the reaction front.

In the early stages of aluminium leaching, after only 15 s in 6 N NaOH at room temperature, two typical situations were observed. In $NiAl_3$ fibres well extracted from the leached aluminium matrix, the reaction front between the unleached $NiAl_3$ and the leached zone (nickel crystallites) was observed, as shown in Fig. 7. Leaching started from the primitive Al–$NiAl_3$ interface and the reaction front remained parallel to the interface. Local EDX microanalysis shows that in the external zone, 1, leaching had extracted the aluminium from the $NiAl_3$ fibres, whereas the internal zone, 2, remained with a high aluminium level. The amount of residual aluminium in the external zone 1, was around 30% (Al/Ni = 0.5). A sharp interface was observed between as-yet unaffected $NiAl_3$ and nickel residue both in images and in composition.

On very thin cross-sections of the $NiAl_3$ fibres, when they were still embedded in the aluminium matrix, a second type of leaching was observed. Fig. 8 shows that aluminium extraction occurred directly from the two free surfaces along the growth direction ⟨0 0 1⟩ of the $NiAl_3$ fibre. In some regions, nickel crystallites were observed surrounded by zones still unleached. These leached zones could be very small (20 nm) and were always elongated in the ⟨1 0 0⟩ direction, parallel to the (0 2 0) planes of the $NiAl_3$ lattice. Moreover, further leaching induced large cracks along these planes in the same direction. It must be noted that no selective aluminium extraction was observed in faceted fibres either in cross-section (Fig. 8), and all the different planes seem reactive with the same degree towards alkali leaching.

At very early stages of leaching, the electron diffraction patterns often appeared with only some enhancement as shown in the inserted pattern presented in Fig. 8. This diffraction pattern shows the unleached

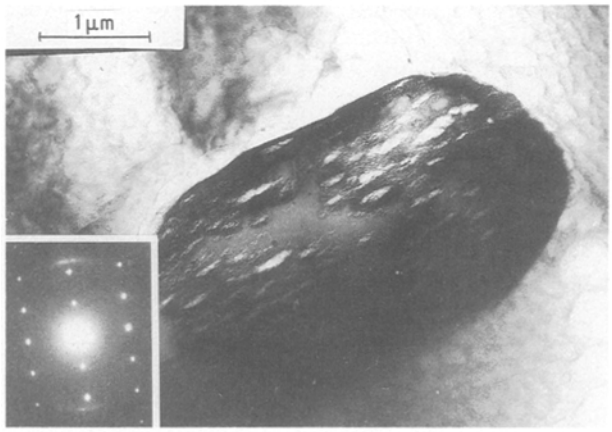

Figure 8 TEM image of the early stages of leaching in an $NiAl_3$ fibre in the ⟨0 0 1⟩ direction. The $NiAl_3$ fibre is oriented in the ⟨0 0 1⟩ direction.

$NiAl_3$ structure along the [0 0 1] direction, and nickel crystallites. These crystallites were oriented at random and moreover, we never observed crystallized nickel particles of smaller size than 3 nm.

During alkali leaching, aluminium in the matrix was extracted as sodium aluminates, soluble in this solution. Indeed on STEM/EDX spectra, the sodium peak remained low (Fig. 9). However, some small areas near the $NiAl_3$ fibres, particularly rich in sodium and aluminium, were analysed indicating a high but not infinite, solubility of $Na(AlO_2)$.

4. Discussion

4.1. Eutectic solidification

The composition of Al/$AlNi_3$ eutectic was first determined by Gwyer in 1908 [16] to be at 6 wt % (2.85 at %) Ni. In the Al–Ni phase diagram, published by

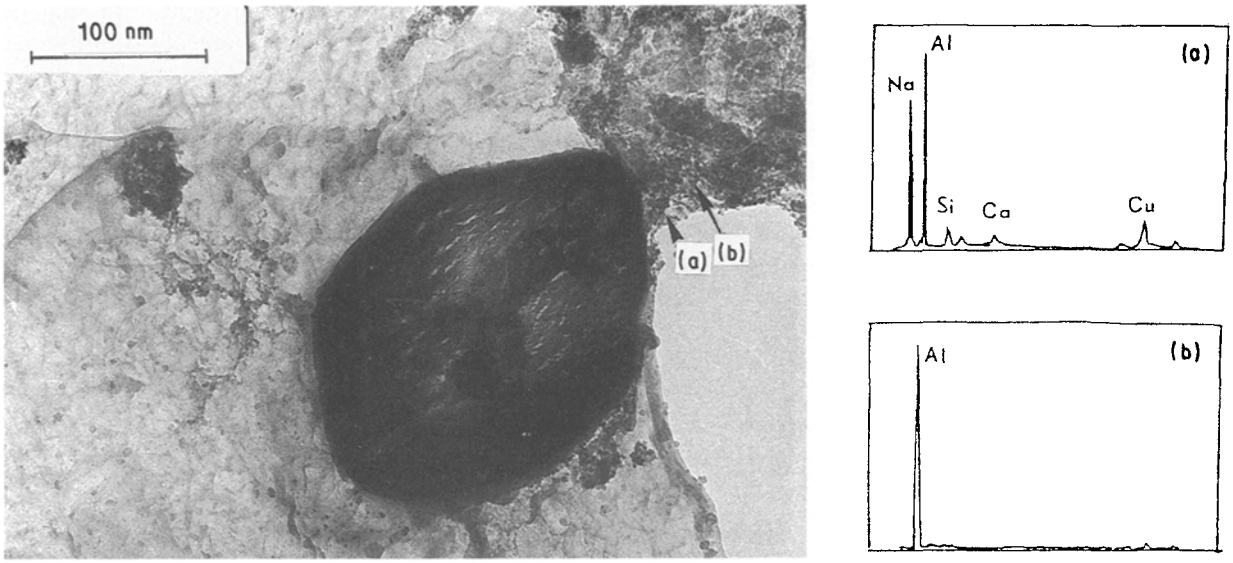

Figure 9 STEM/EDX analysis of the aluminium after alkali leaching, (b), showing that a large amount of sodium can be detected near the $NiAl_3$ fibre (a).

Hansen and Anderko [5] and based on the works of Fink and Willey [17], the eutectic composition was placed at 5.7 wt % (2.7 at %) Ni at 640 °C (913 K). In the 1970s many works were devoted to the relations between the structure and the mechanical properties of this eutectic in order to produce *in situ* composites. The composition was found between 5.3 and 6.3 wt % (2.5 and 3.0 at %) Ni. For Hertzberg *et al.* [14], the coupled eutectic growth occurred in unidirectionally solidified alloys over the composition range 5.64–6.4 wt % Ni. These authors mentioned that in unidirectionally solidified 5.7 wt % Ni alloys performed on large ingots (diameter 2 cm), proeutectic aluminium dendrites were present and the eutectic composition was determined to be around 6.2 wt % Ni. Scheil and Zimmerman [18], and Barclay *et al.* [19] showed that this system exhibited a coupled zone skewed towards the hypereutectic composition. Our observations agree with this skewed coupled zone, with a eutectic composition not included in the coupled region for fast growth rate.

The $Al/NiAl_3$ eutectic microstructure belongs to the fibrous eutectic morphology. As shown by Jackson and Hunt [20], the rod interspacing, λ, was related to the growth rate, R: $\lambda^2 R = a/b$, and an experimental relationship ($\lambda^2 R = 7.7\ \mu m^{3/2}\ s^{-1/2}$) was proposed by Lemkey *et al.* [14] and afterwards used by different authors [19, 21]. The results of Hertzberg *et al.* [14] and Barclay *et al.* [19] are summarized in Fig. 10. As seen in this figure, our results are in agreement with these previous experimental results.

$NiAl_3$ is an isomorph of Ni_3B and Fe_3C, and it is attractive to compare these values with those obtained for the two eutectics, Fe/Fe_3C and Ni/Ni_3B. For these eutectics, the calculated values for $\lambda^2 R$ were 8 [22] and 10 [23] $\mu m^{3/2}\ s^{-1/2}$, respectively. The experimental values are more dispersed in the case of the irregular Fe/Fe_3C eutectic (11–19 $\mu m^{3/2}\ s^{-1/2}$) than in the case of the regular Ni/Ni_3B eutectic (10–12 $\mu m^{3/2}\ s^{-1/2}$). These findings are in agreement

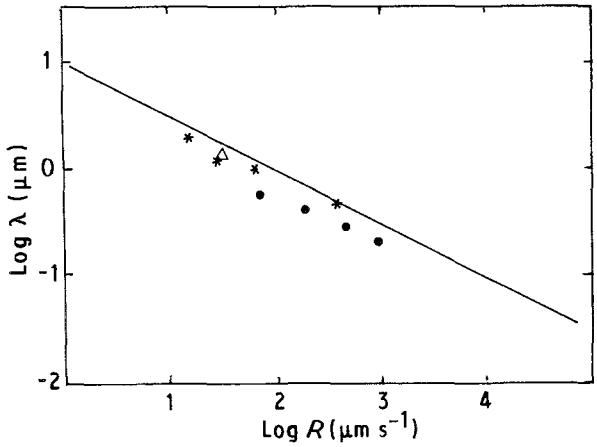

Figure 10 Plot of interfibre spacing, λ, versus growth rate, R: (*) [14, 19]; (△) present work.

with the fact that the eutectic $Al/NiAl_3$ shows essentially regular behaviour.

4.2. Crystallography of the fibrous eutectic Al/Al_3Ni

Several works have dealt with the crystallography of the eutectic and also the anisotropic growth during coarsening. Despite these investigations, there is no consensus regarding the growth direction and the interphase relationships in directionally solidified alloys. The growth direction of the intermetallic phase was always determined around the [0 0 1] direction [14, 24, 25] but the growth direction of aluminium was found around [0 1 1] by some authors [14] and around [2 1 1] by others [24]. For horizontally grown ingots, Jaffrey and Chadwick [25] found no consistent aluminium growth direction. For Cantor and Chadwick [26], a variety of orientations was observed. The orientation of aluminium remains constant but the Al_3Ni fibres are oriented with the [0 0 1]

direction parallel to the fibre axis and to the growth direction.

After annealing treatments, all the authors mentioned that the fibres had developed facets and that the coarsening is anisotropic [24–28]. Jaffrey and Chadwick [25] mentioned that the facets most frequently observed were parallel to either (1 4 0), (1 1 0) and (1 2 0) and minor facets parallel to (2 1 0) and (1 3 0) planes in the $NiAl_3$ lattice. Garmong *et al.* [24] mentioned that the facet planes (3 1 0), (2 1 0) and (1 1 0) changed first with the treatment time, and also with the growth rate in the unidirectionally solidified alloys before heat treatment.

A point to note is that we never observed a unique orientation relationship and that the growth direction of the $NiAl_3$ fibres varied by about 15°. Our results concerning the growth direction of the $NiAl_3$ phase are in agreement with previous results but it seems to be more a mean value than a unique orientation relationship, as proposed by these authors. Moreover, the growth direction of the associated aluminium matrix is around a ⟨0 0 1⟩ direction and therefore completely different from those (⟨1 1 0⟩ or ⟨2 1 1⟩ directions) reported in previous works. No explanation could, in fact, be offered for this discrepancy.

As seen in Figs 3 and 4, $NiAl_3$ fibres generally showed round or elongated shapes but small sets of facets are seen at the edges of the fibres. In our experiments, either in unidirectionally solidified or annealed samples, elongation always occurred along the (0 2 0) planes in the ⟨0 0 1⟩ direction. Our results are in agreement with the majority of previous works reported above.

Bayles *et al.* [29] and Garmong *et al.* [24] discussed the coarsening process in terms of total interfacial energy changes, but these considerations cannot explain the changes of coarsening with time from isotropic to anisotropic.

To understand the faceted structure of the fibres, it must be remembered that a crystal is usually limited by a set of flat faces which forms its morphology. According to the mechanism and the rate of the crystal growth, the morphology of real crystals can be described with two theoretical morphologies [30, 31]. The equilibrium morphology described a state where the surface energies of all the faces of a crystal are in equilibrium either with its vapour or its liquid. The growth morphology is built from the attachment energy of atoms on one face and is directly related to the growth velocity of the face.

From computer calculations [31], the growth morphology of $NiAl_3$ is limited by large (1 1 0), (1 0 1), (1 1 1), (0 2 0) and (2 0 0) faces, while the equilibrium morphology presents a large number of facets (0 1 1), (2 1 1), (1 2 0), (1 0 3), (2 0 0), (2 2 0), (1 1 0) and (0 2 0). In the latter case, the development of (1 2 0) facets is noticeable. In fact, some massive $NiAl_3$ crystals prepared from the melt are limited by planes of the (1 1 0), (1 0 1), (1 1 1) and (0 2 0) types. This morphology is related to the growth morphology [32].

In our eutectic samples, after annealing, two types of fibre were observed. These two types of fibre can be correlated with one of the two types of morphology. In the elongated fibres the (0 2 0) planes are well developed and the (1 1 0) planes are always observed. These fibres are well described by the growth morphology, whereas the small round fibres correspond to the equilibrium morphology where small (1 2 0) facets are effectively detected.

From our observations, the coarsening of the fibres occurs in two steps: first an isotropic coarsening leading to fibres with approximately a two-dimensional equilibrium morphology where the surface energies of all the faces is minimum, then a two-dimensional anisotropic coarsening. In this latter case, the fibres seem to possess a two-dimensional "growth morphology".

These results are in agreement with works of Smartt *et al.* [27]. In fact, these authors mentioned three stages of coarsening of the $NiAl_3$ fibres in the Al/Al_3Ni eutectic. The morphology of the fibres developed during the first stage corresponds to two-dimensional Oswald ripening of the fibres. In Stage III, the breakdown of this stable morphology occurs due to faults in the fibres. This breakdown of stability results in subsequent rapid anisotropic two-dimensional coarsening associated with a two-dimensional "growth morphology". The major and minor ellipse axes do not increase at the same rate. In Stage II, the dimension of the fibres is stable and it seems that mass transfer occurs only when surface diffusion along the fibre circumference restores the equilibrium curvature. This stage seems to correspond to our small fibres showing a two-dimensional "equilibrium morphology".

4.3. Alkali leaching of $NiAl_3$ fibres

From the morphological point of view, fibre morphology is retained after alkali treatment (Fig. 6) and when all the aluminium matrix is dissolved the residue remains in the form of unsupported skeletal fibres as mentioned by Brooks *et al.* [10].

In previous papers, Delannay [33] and the present authors [34] show that Raney nickel catalysts prepared from the Ni_2Al_3 compound consist of nickel crystallites exhibiting preferential orientations with respect to each other. This texture is essentially attributed to the similarity of the structure of NiAl, Ni_2Al_3 and nickel which makes possible a crystallographic transformation between precursor phase Ni_2Al_3 and nickel crystallites. In the case of $NiAl_3$, the porous nickel residue produced by the selective aluminium extraction out of the fibres in the Al/Al_3Ni eutectic shows no direct orientation relationship between the $NiAl_3$ precursor phase and the nickel crystallites (Fig. 6). This observation is related to the absence of a simple crystallographic relation between the orthorhombic $NiAl_3$ and the f c c nickel cell lattices.

Another interesting point to follow is the early stage of the leaching reaction. From Figs 5 and 7, the aluminium extraction of the eutectic structure occurred in two steps:

(i) first the aluminium matrix, very reactive towards alkali solution, begins to be leached, then

(ii) aluminium is extracted from the $NiAl_3$ fibres. This aluminium extraction of the intermetallic $NiAl_3$ compound followed two processes. In the thinnest zones of the $NiAl_3$ phase, aluminium leaching occurred directly from the alkali solution. If the zones to be leached are too thick, $NiAl_3$ would only be leached if the surrounding aluminium matrix is previously leached.

In the latter case, the reaction front between the leached (where nickel crystallites are detected) and the unleached zones remains almost parallel to the primitive Al/Al_3Ni interface (Fig. 7). The nickel crystallites are detectable from TEM images only if the aluminium level is below 30 at %. This value was larger than the solubility limit of aluminium in nickel (10 at % at room temperature) but corresponds approximately to the limit of the two-phase domains $Ni + Ni_3Al$. In the inner region, the aluminium level (about 75 at %) corresponds to the unleached $NiAl_3$ phase.

In very thin samples, aluminium leaching out of the $NiAl_3$ phase occurs directly from the alkali solution. As shown in Fig. 8, aluminium extraction first occurs along the ⟨0 0 1⟩ direction, then the propagation of the leaching occurs along the (0 2 0) planes where cracks are effectively observed. The structure of $NiAl_3$ belongs to the space group Pbnm and the projection along the [1 0 0] direction is presented in Fig. 11. The local environment around a nickel atom is constructed from a trigonal prism of six aluminium atoms. Along the ⟨1 0 0⟩ direction large voids exist between these prisms and, moreover, wavy layers of aluminium atoms are very clear. Therefore, it seems possible to introduce OH^- atoms and extract aluminium atoms along the ⟨0 0 1⟩ direction. Owing to the pleated aluminium atom layers parallel to the (0 1 0) planes, the propagation of leaching seems easier along this (0 1 0) plane.

During these early stages of leaching, only rings of an fcc cell are detectable in electron diffraction patterns and for longer leaching times, nickel reflections begin to appear. The nickel reflections indexed as shown in Fig. 5 are observed after restructuring and sintering of smaller nickel crystallites have occurred during leaching.

Bakker *et al.* [12] show that the behaviour during leaching of the phases Ni_2Al_3 and $NiAl_3$ is very different. The leaching of $NiAl_3$ leads to a nickel residue which tends to disintegrate while the reaction product formed from Ni_2Al_3 appears in a strong aggregate form. As reported by different authors for the primary $NiAl_3$ phase [12], leaching of the $NiAl_3$ in the eutectic fibres occurs with the formation of cracks. Two assumptions were proposed: the cracks are produced because the nickel residue is friable, and no protective layer on the surface of the nickel residue can be formed due to gas evolution. During further leaching, sintering of the nickel crystallites occurs and the volume fraction of nickel in the leached residue is smaller than the volume of the precursor phase, leading to a large void fraction inducing cracks.

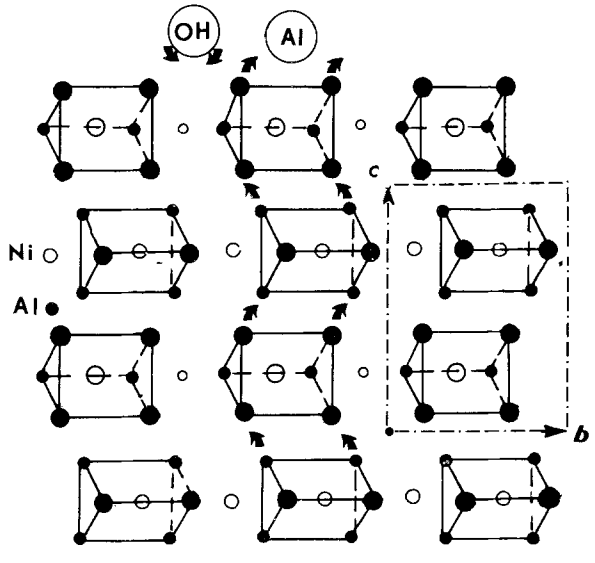

Figure 11 Projection along the [1 0 0] axis for $NiAl_3$ showing wavy layers of aluminium atoms and the voids between these layers allowing OH^- introduction and aluminium extraction.

5. Conclusion

Our aim was to study at fine scale the metallurgical structure of Al/Al_3Ni eutectic, in order to understand the preparation of nickel catalysts from these precursor alloys. The fibrous eutectic was regular and some faceting of the $NiAl_3$ fibres was observed after heat treatment.

After alkali leaching, the fibrous morphology was retained. Aluminium leaching of $NiAl_3$ phase occurred in two typical ways: from the external interface between aluminium and $NiAl_3$, and directly in the $NiAl_3$ phase along the ⟨0 0 1⟩ direction.

Acknowledgements

This study was supported by the Unite Mixte Rhone-Poulenc-CNRS. One of the authors (P.C.) thanks U.M. for financial support.

References

1. R. SASSOUSLAS and Y. TRAMBBOUZE, *Bull. Soc. Chim. Fr.* **5** (1964) 985.
2. M. KHAIDAR, C. ALLIBERT and J. DRIOLE, *Mater. Res. Bull.* **17** (1982) 329.
3. A. B. FASMAN, S. D. MIKHAILENKO, N. A. MARKSIMOVA, Zh. A. IKHSANOV, V. Y. KITAIGORODSKAYA and L. V. PAVLYKEVITCH, *Appl. Catal.* **6** (1983) 1.
4. J. GROS, S. HAMAR-THIBAULT and J. C. JOUD, *J. Mater. Sci.* **24** (1989) 2987.
5. M. HANSEN and A. ANDERKO, "Constitution of Binary Alloys" (McGraw-Hill, New York, 1958).
6. J. FREEL, W. J. M. PIETERS and R. B. ANDERSON, *J. Catal.* **14** (1968) 247.
7. L. L. ODEN and J. H. RUSSEL, US Bureau of Mines, Report of Investigations 8272 (1978).
8. P. FOUILLOUX, *Appl. Catal.* **8** (1983) 1.
9. S. SANE, J. M. BONNIER, J. P. DAMON and J. MASSON, *ibid.* **9** (1984) 69.
10. C. S. BROOKS, F. D. LEMKEY and G. S. GOLDEN, in "Proceedings of the 3rd Conference on *in situ* Composites", edited by H. Bibring, J. L. Walter and B. F. Olivier (Custom, Lexington, MA, 1979) p. 221.
11. F. D. LEMKEY and G. S. GOLDEN, US Pat. 4086 (1978) p. 264.

12. M. L. BAKKER, D. J. YOUNG and M. S. WAINWRIGHT, *J. Mater. Sci.* **23** (1988) 3921.
13. M. DURAND-CHARRE, G. MARCON, G. MASSARD and F. DURAND, *J. Less-Common Metals* **32** (1973) 103.
14. R. W. HERTZBERG, F. D. LEMKEY and J. A. FORD, *Trans. TMS-AIME* **233** (1965) 334.
15. C. J. SMITHELLS, "Metals Reference Book" (Butterworths, London, 1955).
16. A. G. C. GWYER, *Z. Anorg. Chem.* **57** (1908) 133.
17. W. L. FINK and L. A. WILLEY, *Trans. TMS-AIME* **111** (1934) 293.
18. E. SCHIEL and R. ZIMMERMAN, *Z. Metallkde* **48** (1957) 509.
19. R. S. BARCLAY, H. W. KERR and P. NIESSEN, *J. Mater. Sci.* **6** (1971) 1168.
20. K. A. JACKSON and J. D. HUNT, *Trans. TMS-AIME* **236** (1966) 112.
21. M. M. FARAG and M. C. FLEMMINGS, *Met. Trans.* **7A** (1976) 215.
22. H. JONES and W. KURZ, *Z. Metallkde* **72** (1981) 792.
23. J. AJAO and S. HAMAR-THIBAULT, *J. Mater. Sci.* **23** (1988) 1112.
24. G. GARMONG, C. G. RHODES and R. A. SPURLING, *Met. Trans.* **4** (1973) 707.
25. D. JAFFREY and G. A. CHADWICK, *ibid.* **1** (1970) 3389.
26. B. CANTOR and G. A. CHADWICK, *J. Crystal Growth* **30** (1975) 101.
27. H. B. SMARTT, L. K. TU and T. H. COURTNEY, *Met. Trans.* **2A** (1971) 2717.
28. H. B. SMARTT and T. H. COURTNEY, *ibid.* **7A** (1976) 123.
29. B. J. BAYLES, F. A. FORD and M. J. SALKIND, *Trans. TMS-AIME* **239** (1967) 844.
30. P. HARTMAN, in "Crystal Growth: an Introduction", edited by P. Hartman (North-Holland, Amsterdam, 1973) p. 367.
31. R. HAMAR, private communication (1990).
32. D. TASSONI, J. P. RIQUET and F. DURAND, *Acta Crystallogr.* **36A** (1980) 420.
33. F. DELANNAY, *Reactiv. Solids* **2** (1986) 235.
34. J. GROS, S. HAMAR-THIBAULT and J. C. JOUD, *Surface Interface Anal.* **11** (1988) 611.

Received 5 November 1990
and accepted 25 March 1991